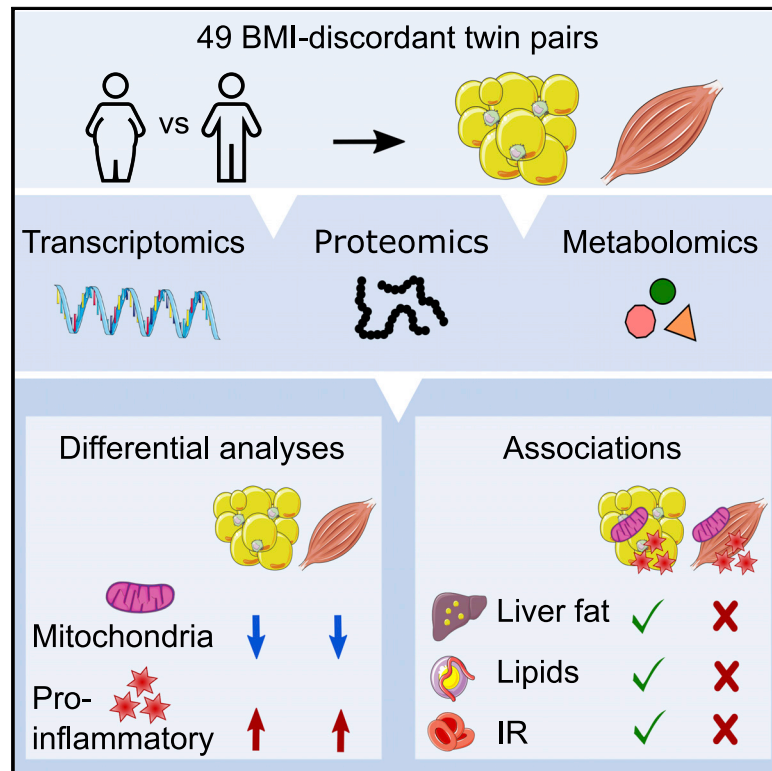**Article**

Molecular pathways behind acquired obesity: Adipose tissue and skeletal muscle multiomics in monozygotic twin pairs discordant for BMI

Graphical abstract

Authors

Birgitta W. van der Kolk, Sina Saari, Alen Lovric, ..., Adil Mardinoglu, Päivi Pajukanta, Kirsi H. Pietiläinen

Correspondence

birgitta.vanderkolk@helsinki.fi (B.W.v.d.K.),
kirsi.pietilainen@helsinki.fi (K.H.P.)

In brief

In adipose tissue and skeletal muscle of BMI-discordant monozygotic twin pairs, van der Kolk et al. demonstrate that excess body weight is associated with downregulated mitochondrial pathways and upregulated proinflammatory pathways. Furthermore, adipose tissue metabolic alterations appear to be more pronounced than those in muscle, whereas only adipose tissue alterations are associated with metabolic health.

Highlights

- Multiomics analyses of adipose tissue and skeletal muscle in BMI-discordant twins

- Excess body weight downregulates mitochondrial pathways in both tissues

- Excess body weight upregulates proinflammatory pathways in both tissues

- Adipose tissue alterations are associated with metabolic health in acquired obesity

CellPress

Cell Reports Medicine

Article

Molecular pathways behind acquired obesity: Adipose tissue and skeletal muscle multiomics in monozygotic twin pairs discordant for BMI

Birgitta W. van der Kolk,[1,19,*] Sina Saari,[1,19] Alen Lovric,[2,3] Muhammad Arif,[2] Marcus Alvarez,[4] Arthur Ko,[5] Zong Miao,[4,6] Navid Sahebekhtiari,[1] Maheswary Muniandy,[1] Sini Heinonen,[1] Ali Oghabian,[1] Riikka Jokinen,[1] Sakari Jukarainen,[7] Antti Hakkarainen,[8] Jesper Lundbom,[8,9] Juho Kuula,[8,10] Per-Henrik Groop,[11,12,13,14] Taru Tukiainen,[7] Nina Lundbom,[8] Aila Rissanen,[1] Jaakko Kaprio,[7] Evan G. Williams,[15] Nicola Zamboni,[15] Adil Mardinoglu,[2,16] Päivi Pajukanta,[4,6,17] and Kirsi H. Pietiläinen[1,18,20,*]

[1]Obesity Research Unit, Research Program for Clinical and Molecular Metabolism, Faculty of Medicine, University of Helsinki, Helsinki, Finland
[2]Science for Life Laboratory, KTH-Royal Institute of Technology, Stockholm, Sweden
[3]Division of Clinical Physiology, Department of Laboratory Medicine, Karolinska Institutet and Unit of Clinical Physiology, Karolinska University Hospital, Stockholm, Sweden
[4]Department of Human Genetics, David Geffen School of Medicine, University of California, Los Angeles, Los Angeles, CA, USA
[5]Department of Medicine, David Geffen School of Medicine, University of California, Los Angeles, Los Angeles, CA, USA
[6]Bioinformatics Interdepartmental Program, University of California, Los Angeles, Los Angeles, CA, USA
[7]Institute for Molecular Medicine Finland, FIMM, University of Helsinki, Helsinki, Finland
[8]HUS Medical Imaging Center, Radiology, University of Helsinki and Helsinki University Hospital, Helsinki, Finland
[9]Institute for Clinical Diabetology, German Diabetes Center, Leibniz Center for Diabetes Research, Heinrich Heine University, Düsseldorf, Germany
[10]Public Health Promotion Unit, National Institute for Health and Welfare, Helsinki, Finland
[11]Folkhälsan Institute of Genetics, Folkhälsan Research Center, Helsinki, Finland
[12]Research Program for Clinical and Molecular Metabolism, Faculty of Medicine, University of Helsinki, Helsinki, Finland
[13]Abdominal Center, Nephrology, University of Helsinki and Helsinki University Hospital, Helsinki, Finland
[14]Department of Diabetes, Central Clinical School, Monash University, Melbourne, VIC, Australia
[15]Institute of Molecular Systems Biology, ETH Zurich, Zurich, Switzerland
[16]Centre for Host-Microbiome Interactions, Dental Institute, King's College London, London, UK
[17]Institute for Precision Health, David Geffen School of Medicine, University of California, Los Angeles, Los Angeles, CA, USA
[18]Obesity Center, Abdominal Center, Helsinki University Hospital, Helsinki, Finland
[19]These authors contributed equally
[20]Lead contact
*Correspondence: birgitta.vanderkolk@helsinki.fi (B.W.v.d.K.), kirsi.pietilainen@helsinki.fi (K.H.P.)
https://doi.org/10.1016/j.xcrm.2021.100226

SUMMARY

Tissue-specific mechanisms prompting obesity-related development complications in humans remain unclear. We apply multiomics analyses of subcutaneous adipose tissue and skeletal muscle to examine the effects of acquired obesity among 49 BMI-discordant monozygotic twin pairs. Overall, adipose tissue appears to be more affected by excess body weight than skeletal muscle. In heavier co-twins, we observe a transcriptional pattern of downregulated mitochondrial pathways in both tissues and upregulated inflammatory pathways in adipose tissue. In adipose tissue, heavier co-twins exhibit lower creatine levels; in skeletal muscle, glycolysis- and redox stress-related protein and metabolite levels remain higher. Furthermore, metabolomics analyses in both tissues reveal that several proinflammatory lipids are higher and six of the same lipid derivatives are lower in acquired obesity. Finally, in adipose tissue, but not in skeletal muscle, mitochondrial downregulation and upregulated inflammation are associated with a fatty liver, insulin resistance, and dyslipidemia, suggesting that adipose tissue dominates in acquired obesity.

INTRODUCTION

Obesity, a major public health burden, has increased globally, doubling in prevalence in 70 countries between 1980 and 2015.[1] Obesity predisposes individuals to a range of complex metabolic diseases, including type 2 diabetes mellitus (T2DM), cardiovascular diseases, and some cancers.[2] Triggers for obesity and related adverse health outcomes vary remarkably between individuals and are multifactorial, involving genetic and lifestyle factors in the context of multiple social and environmental changes.

Table 1. Participant characteristics of 49 monozygotic twin pairs discordant for BMI with a mean age of 45.7 years (SD ± 17.8); 27 pairs (55%) were female

	Leaner Co-twin	Heavier Co-twin	p Value
Body weight (kg)	75.8 ± 15.6	92.7 ± 17.9	<0.001
BMI (kg/m^2)	26.2 ± 4.7	32.0 ± 5.5	<0.001
Body fat (%)	33.5 ± 9.0	41.1 ± 7.3	<0.001
Body fat (kg)	26.7 ± 10.9	39.0 ± 11.6	<0.001
Fat-free mass (kg)	47.5 ± 9.9	51.2 ± 11.7	<0.001
Subcutaneous fat (cm^3)[a]	3,013 (2,435–4,697)	5,527 (4,312–7,652)	<0.001
Intra-abdominal fat (cm^3)[a]	552 (327–805)	1,146 (743–2214)	<0.001
Adipocyte volume (pl)	450 ± 192	637 ± 232	<0.001
Liver fat (%)[a]	0.6 (0.4–1.1)	2.7 (0.7–8.2)	<0.001
Fasting glucose (mmol/L)	5.5 (5.0–5.8)	5.8 (5.2–6.0)	0.028
Fasting insulin (mU/L)	5.3 (3.3–7.3)	7.9 (5.4–12.4)	<0.001
HOMA-IR index	1.1 (0.7–1.7)	2.0 (1.5–3.1)	<0.001
Matsuda index	7.2 (4.7–9.6)	4.0 (2.7–5.2)	<0.001
Total cholesterol (mmol/L)	4.8 ± 0.9	4.9 ± 1.0	0.401
HDL cholesterol (mmol/L)	1.6 (1.3–1.9)	1.4 (1.2–1.7)	<0.001
LDL cholesterol (mmol/L)	2.9 ± 0.8	3.1 ± 0.9	0.117
Triacylglycerol (mmol/L)	0.9 (0.7–1.1)	1.3 (0.9–1.3)	<0.001
CRP (mg/L)	1.4 (0.6–4.0)	1.7 (0.9–3.7)	0.182
Total physical activity (Baecke)	8.4 (7.0–9.3)	7.9 (6.9–9.0)	0.350

Data are reported as mean ± SD (normally distributed variables) or median (interquartile range for skewed variables). We used paired t tests to calculate the p values and considered p < 0.05 significant. Skewed variables were log$_e$ transformed before analysis. BMI, body mass index; HDL, high-density lipoprotein; LDL, low-density lipoprotein; HOMA-IR, homeostatic model for the assessment of insulin resistance; CRP, C-reactive protein.
[a]Data are based on 26 twin pairs.

Obesity affects key metabolic organs, including adipose tissue and skeletal muscle, closely associated with metabolic health.[3] Dysfunction of excess adipose tissue is characterized by increased adipocyte size (hypertrophy),[4] downregulation of mitochondrial oxidative metabolism,[5] impaired lipid buffering capacity,[6] and increased inflammation.[7] Consequently, ectopic lipid accumulation (because of saturation of adipose tissue storage capacity), mitochondrial dysregulation, and low-grade inflammation may contribute to development of skeletal muscle and liver dysfunction, including diminished insulin sensitivity and increased oxidative stress and inflammation.[6,8]

To date, few global omics studies have examined adipose tissue and skeletal muscle separately to unravel the metabolic alterations associated with obesity. Global transcriptomics studies have shown significant adipose tissue dysregulation in obesity and insulin resistance. The adipose tissue transcriptome is characterized by downregulation of mitochondrion-related pathways, including oxidative phosphorylation (OXPHOS), branched-chain amino acid (BCAA) catabolism, fatty acid

β-oxidation,[9–11] and upregulation of inflammatory[9–13] and extracellular matrix organization pathways.[12,13] These findings become more distinct among individuals with more pronounced insulin resistance.[11,13–15] Furthermore, microarray analyses of mature adipocytes[16–18] and metabolomics of adipose stem cell cultures[19] also revealed alterations in glucose and amino acid metabolism, mitochondrial metabolism, and inflammation in obesity.

In skeletal muscle tissue, several single omics analyses have been performed, although they primarily focused on insulin resistance and T2DM rather than obesity per se. Skeletal muscle transcriptome analyses[20,21] and transcriptome analyses from isolated myoblasts[22] from individuals with T2DM compared with healthy controls identified downregulation of mitochondrial pathways and myogenesis[20–22] and upregulation of apoptosis and inflammation.[21] Similarly, in T2DM, lower mitochondrial and amino acid metabolism protein levels and higher glycolysis- and stress-related protein levels were found using proteomics platforms.[23–27] Less is known about perturbations in skeletal muscle tissue metabolism in obesity without metabolic complications, although smaller proteomics studies suggest lower mitochondrial protein levels in obesity even in the absence of T2DM.[24–27]

To date, several studies have combined metabolic tissue and/or plasma collections to identify biomarkers of insulin resistance or T2DM,[28–35] but only a few have specifically studied obesity. A comprehensive global understanding of the underlying mechanisms of obesity and the early stages of metabolic complications at the whole-body and tissue-specific level is currently lacking. Furthermore, the relative importance of adipose tissue and skeletal muscle for development of concomitant complications in obesity remains unclear, as do the roles of genetics and lifestyle factors affecting obesity in tissue metabolism.

Here we aimed to understand the tissue-specific biological mechanisms and the relative tissue-specific importance underlying acquired obesity and related metabolic alterations. We apply a multiomics framework to adipose tissue and skeletal muscle by examining biological networks constructed using RNA sequencing, proteomics, and metabolomics obtained from 49 rare monozygotic twin pairs discordant for body mass index (BMI); that is, when one twin is heavier than their co-twin. These individuals share a genetic background as well as most early life events and a family environment. Thus, our results provide a global metabolic profile in obesity primarily dependent upon acquired, environmental, and lifestyle factors.

RESULTS

Twin pairs highly discordant for clinical characteristics of obesity

Table 1 summarizes the anthropometric and metabolic characteristics of leaner and heavier co-twins. The twin pairs, with a mean weight difference of 17.1 ± 9.0 kg, were highly discordant (p < 0.001) for all measures of adiposity. In addition, the heavier co-twins were more insulin resistant (p < 0.001) with higher plasma triacylglycerol (TAG) concentrations (p < 0.001) and lower levels of high-density lipoprotein (HDL) (p < 0.001), whereas the fasting glucose level was only marginally higher in the heavier twin

(p = 0.028). We detected no differences in total cholesterol, low-density lipoprotein (LDL) cholesterol, C-reactive protein (CRP), or physical activity levels between the heavier and leaner co-twins.

More transcripts were altered in adipose tissue than in skeletal muscle

To understand the biological effect of the acquired excess body weight, we first compared the adipose tissue and skeletal muscle transcriptomes among co-twins. In adipose tissue, among 14,558 identified genes, 3,454 transcripts were expressed differentially between co-twins (false discovery rate [FDR] p < 0.05), with a total of 1,615 downregulated and 1,839 upregulated genes in the heavier co-twins (Table S1). The top 50 downregulated differentially expressed genes included mitochondrial metabolism-related genes (e.g., *ACSS3*, *ETFA*, *MCCC2*, and *PCCA*) and lipid metabolism genes (*SLC27A2*, *LPIN1*, *PPARA*, *HADH*, and *CIDEA*). The top 50 upregulated genes included inflammation-related genes (*IL1RN*, *C3AR1*, *CMSD2*, and *CD163*).

In skeletal muscle, among 13,179 identified genes, we identified 1,287 differentially expressed genes between co-twins (nominal p < 0.05, four genes with FDR p < 0.05), of which 665 were downregulated and 622 were upregulated in the heavier co-twins (Table S2). The top 50 downregulated genes included growth and nutrient-sensing genes (*AKT1* and *PDE4A*) and mitochondrial membrane transport genes (*HK2* and *MCUR1*). The top 50 upregulated genes were linked to oxidoreductase activity (*NQO1*) and lipid metabolism (*THRSP* and *TYSND1*).

KEGG pathway enrichment alterations in adipose tissue and skeletal muscle

To gain insight into the differentially expressed transcriptome in adipose tissue and skeletal muscle, we performed KEGG (Kyoto Encyclopedia of Genes and Genomes) pathway enrichment analyses. We observed consistent downregulation of mitochondrion-related metabolic pathways in the heavier co-twins in adipose tissue and skeletal muscle (Figure 1A). Upregulated pathways in adipose and skeletal muscle tissue included the extracellular matrix (ECM) remodeling pathways (Figure 1A).

In adipose tissue, we found multiple fatty acid metabolism pathways, linked to lipid degradation among the most downregulated pathways. Twenty-two inflammatory pathways were upregulated significantly in the heavier co-twin (Figure 1B), including pathways related to innate and adaptive inflammation, such as the complement and coagulation cascades and Toll-like receptor signaling and T cell receptor signaling pathways. Other upregulated pathways were associated primarily with cell signaling.

In skeletal muscle tissue, we found 12 significantly different pathways in co-twins (Figure 1C). Nutrient-sensing pathways, including the insulin signaling pathway and autophagy, were downregulated in the heavier co-twin along with metabolism of several amino acids. The upregulated pathways in the skeletal muscle tissue were involved in the N-glycan biosynthesis pathway.

Downregulated transcripts for most genes in mitochondrion-related pathways

Next, because mitochondrion-related metabolic pathways were downregulated in both tissues, we inspected the individual tran-scripts of the significantly differentially expressed mitochondrial pathways (Figure 1): OXPHOS, tricarboxylic acid (TCA) cycle, pyruvate metabolism, and BCAA (i.e., valine, leucine, and isoleucine) degradation. The overall pattern clearly revealed that all five complexes of OXPHOS were downregulated in adipose and skeletal muscle tissue in the heavier co-twins (Figure 2). The majority of TCA cycle-related, pyruvate metabolism, and BCAA degradation genes tended toward downregulation in the heavier co-twins in both tissues (Figure 2). Notable exceptions included the upregulated cytosolic genes *BCAT1* and *SDS* in adipose tissue, which control BCAA degradation before mitochondrial oxidation.

Reporter metabolite analysis predicts alterations in mitochondrial metabolites

We integrated the RNA sequencing data with genome-scale metabolic models to gain insight into the subcellular localization of the altered metabolic reactions as well as the reporter metabolites between co-twins.[36,37] In adipose tissue, most of the reporter metabolites affected by transcriptional downregulation in the heavier co-twin were mitochondrial (Figure 3A). Skeletal muscle showed a similar, although less prominent pattern for mitochondrial reporter metabolites associated with transcriptional downregulation (Figure 3A). The reporter metabolites associated with the transcriptional upregulation localized to the lysosomes and Golgi apparatus for adipose tissue and skeletal muscle (Figure 3A).

We then selected individual reporter metabolites (based on the Metabolic Atlas[38]) involved in the significantly altered mitochondrial pathways, as shown in Figure 2. We found that the majority of significantly altered reporter metabolites appeared in adipose tissue (Figure 3B). For both tissues, significant reporter metabolites in the mitochondrial pathways were transcriptionally downregulated in the heavier co-twins, with the exception of citrate [c] for skeletal muscle, which was upregulated in the heavier co-twins. The majority of OXPHOS and TCA cycle intermediates were transcriptionally downregulated in the heavier co-twin in adipose tissue. Pyruvate emerged as transcriptionally downregulated in both tissues, particularly the downstream genes. BCAA reporter metabolites were also identified as transcriptionally downregulated, especially in adipose tissue. In summary, adipose tissue exhibited a higher number of affected reporter metabolites and, in both tissues, significant downregulation of genes around OXPHOS, the TCA cycle, pyruvate, and BCAA occurred in the heavier co-twins.

Tissue metabolomics alterations in adipose tissue and skeletal muscle

To characterize the actual metabolome in acquired obesity, we applied an untargeted metabolomics approach using mass spectrometry, identifying 1,391 metabolites. In adipose tissue, 17 of 37 significantly altered metabolites (Table S3) and 21 of 63 significantly altered metabolites in skeletal muscle tissue (Table S3) were lower in the heavier co-twins. Six lipid-related metabolites were significantly lower in both tissues in the heavier co-twins, including two oxylipins (Table S3).

In adipose tissue, metabolites with lower levels in the heavier co-twins also included creatine, ATP, and taurocholic acid. The
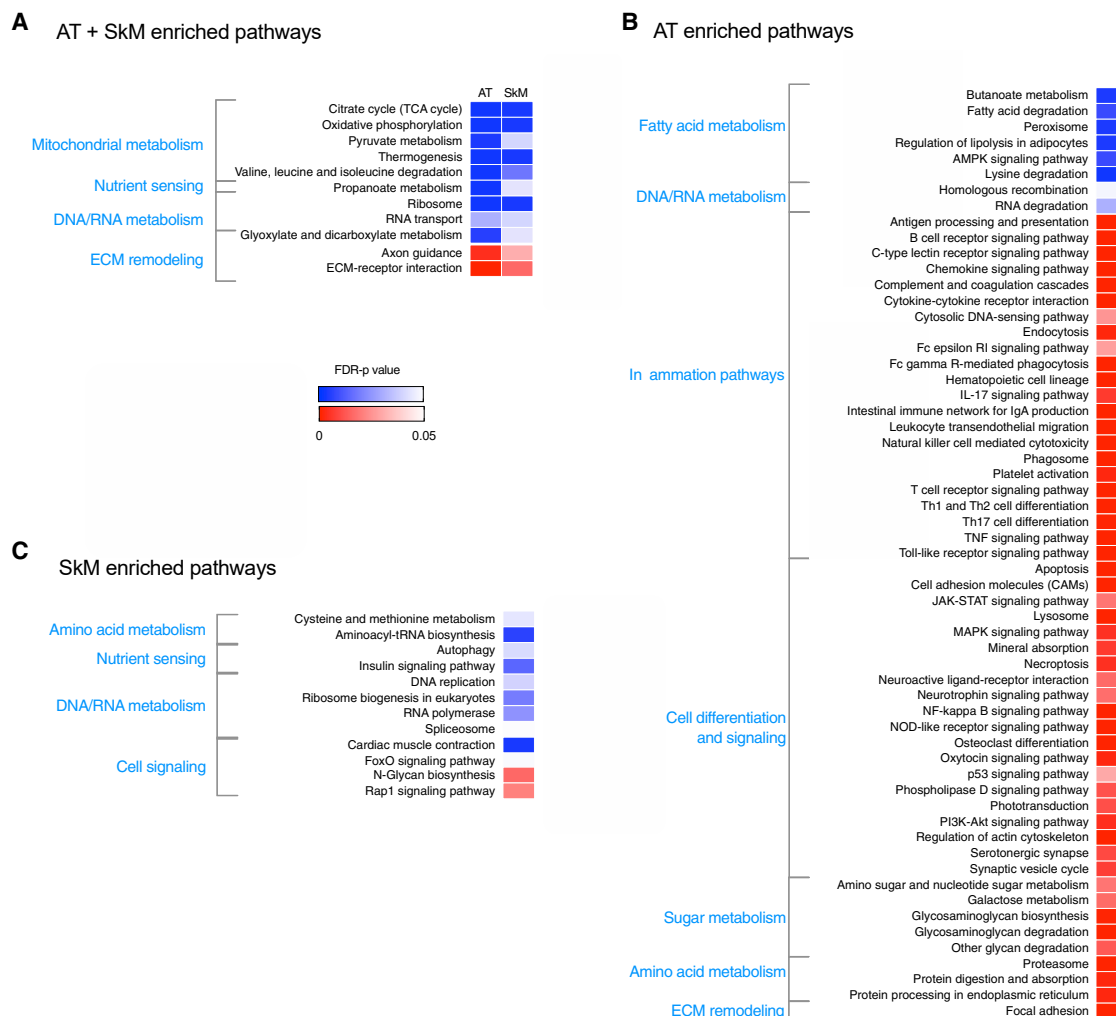
Figure 1. KEGG pathway enrichment analysis of differentially expressed genes in co-twins

(A) The heatmap presents pathways that are significantly different in both tissues.

(B) The heatmap presents significantly altered pathways in adipose tissue (n = 49 twin pairs).

(C) The heatmap presents significantly altered pathways in skeletal muscle (n = 44 twin pairs).

The direction and significance of each pathway was based on the gene set as a whole while considering the p value and fold change for each gene. KEGG pathways with FDR p < 0.05 are shown; blue indicates significantly downregulated pathways in the heavier co-twins, whereas red indicates upregulated pathways. Pathways are grouped according to their biological function. AT, adipose tissue; SkM, skeletal muscle; ECM, extracellular matrix.

most significantly altered metabolite at higher levels consisted of the ceramide species C18:Cer (Table S3).

In skeletal muscle, lower levels of metabolites in the heavier co-twins were associated primarily with a variety of lipid intermediates (Table S3). Pyruvate emerged as the most significantly altered metabolite, exhibiting higher levels in the heavier co-twins, followed by several proinflammatory polyunsaturated fatty acid-related eicosanoids (eicosadienoic acid, arachidonic acid, leukotriene A4, and prostaglandin derivatives).

Comparison of mitochondrial metabolism in predicted reporter and actual metabolites

Next, for the mitochondrial pathways, we compared the actual metabolome results with the genome-scale metabolic models

results; that is, the reporter metabolites. We only identified two significantly different metabolites in the mitochondrial pathways between co-twins. In adipose tissue, ATP levels were lower in the heavier co-twins (Figure 4B), consistent with the reporter metabolite analysis. In skeletal muscle, we observed a transcriptional alteration around pyruvate in the reporter metabolite analysis, which we confirmed with untargeted metabolomics, in which pyruvate levels were higher in the heavier twins (Figure 4A). Interestingly, we observed higher TCA intermediate levels downstream of pyruvate until α-keto-glutarate in skeletal muscle (Figure 4A), whereas in adipose tissue, the actual metabolome results point toward a consistent pattern of lower TCA intermediate levels (Figure 4A), a pattern also suggested by the reporter metabolite analysis.
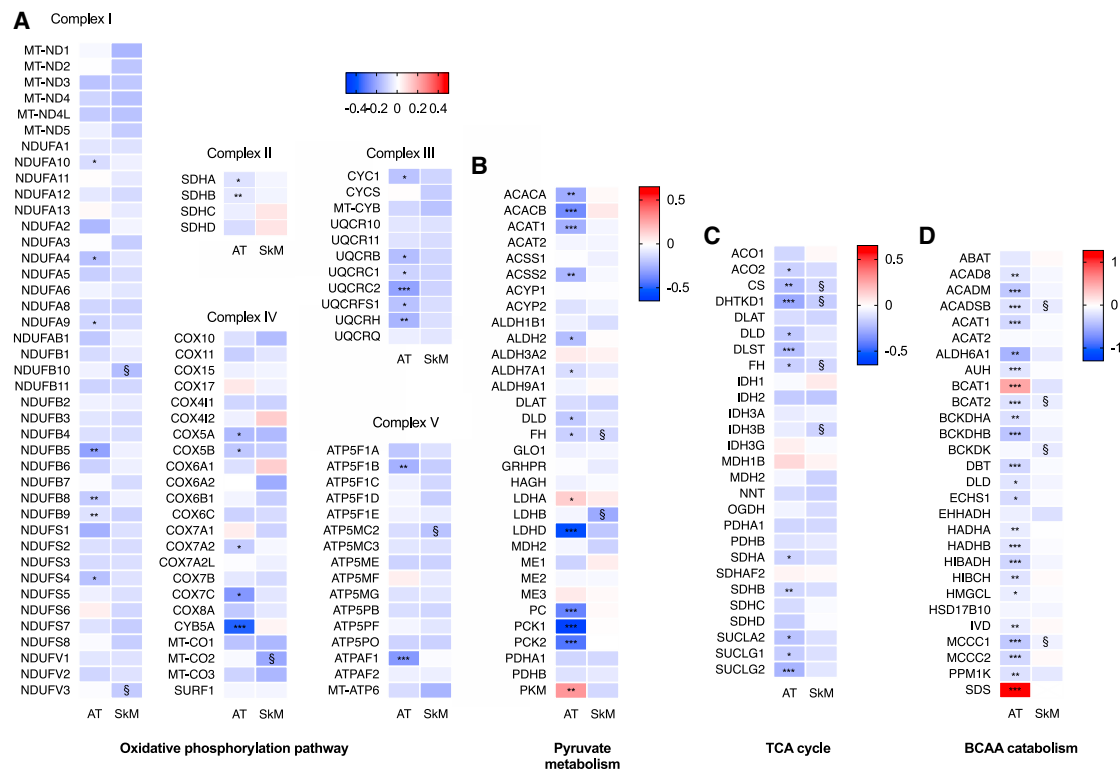
Figure 2. Heatmaps showing the differential expression of individual genes in four mitochondrial pathways among co-twins

The heatmaps show the downregulation in transcription levels for the majority of genes involved in the central mitochondrial pathways in AT (n = 49 twin pairs) and SkM (n = 44 twin pairs). The $\log_2$-fold differences indicated for the genes are based on the KEGG pathways. The color in the heatmaps reflects the differential expressions associated with the heavier co-twins, where blue indicates downregulation and red indicates upregulation. Asterisks indicate statistically significant differential expression: ***FDR $p < 0.001$, **FDR $p < 0.01$, *FDR $p < 0.05$, §nominal $p < 0.05$. TCA, tricarboxylic acid; BCAA, branched-chain amino acids.

Nevertheless, the TCA or BCAA metabolites (Figure 4C) between leaner and heavier co-twins were not significantly different in either tissue.

Differences in the skeletal muscle proteome related to glycolysis and oxidative stress pathways

We also assessed the skeletal muscle proteome. We identified 881 proteins, 43 of which were significantly different between co-twins (nominal $p < 0.05$; Table S4). Seven proteins had lower expression levels in the heavier co-twins, including the mitochondrial outer membrane protein CISD1 and two proteins involved in cytoskeleton organization, FLNB and MYL6B. The 36 proteins with a higher expression level in the heavier co-twin were involved in stress and redox homeostasis (PARK7, GLRX, and HSP90), generating pyruvate through glycolysis (PFKP, PFKM, and PGK2), and converting pyruvate to lactate (LDHA). The KEGG pathway enrichment analyses indicated glycolysis (LDHA, PFKP, PFKM, and PGK2) as the most significantly altered pathway (Table S5). The proteomics results point toward a consistent pattern of higher levels of glycolytic proteins in skeletal muscle (Figure 4D), although we only identified a few that were significantly different between co-twins.

Adipose tissue mitochondrial and inflammatory pathways related to metabolic health

Following the transcriptome analyses in adipose tissue and skeletal muscle, we studied the relationship between four mitochondrial pathways (OXPHOS, the TCA cycle, pyruvate metabolism, and BCAA degradation), three inflammation pathways (complement and coagulation cascade, phagosome, and T cell receptor signaling pathways), and clinical outcomes among co-twins.

A combined score for genes in the mitochondrial pathways was consistently associated negatively with multiple measures for adiposity, such as subcutaneous adipose tissue volume and the percentage of liver fat, insulin resistance (i.e., negatively with the homeostatic model for the assessment of insulin resistance (HOMA-IR) and positively with the Matsuda index), and TAG and CRP in adipose tissue. However, we observed no such associations with skeletal muscle (Figure 5). These correlations were significant for the adiposity measures and tended to be significant for insulin sensitivity measures when using the within-pair differences for the measures; that is, controlling for genetic influence (Figure 5). When analyzing twins as individuals, all of these correlations were significant (Figure S1).

For the complement and coagulation cascade and phagosome pathways, we observed a consistent pattern of positive
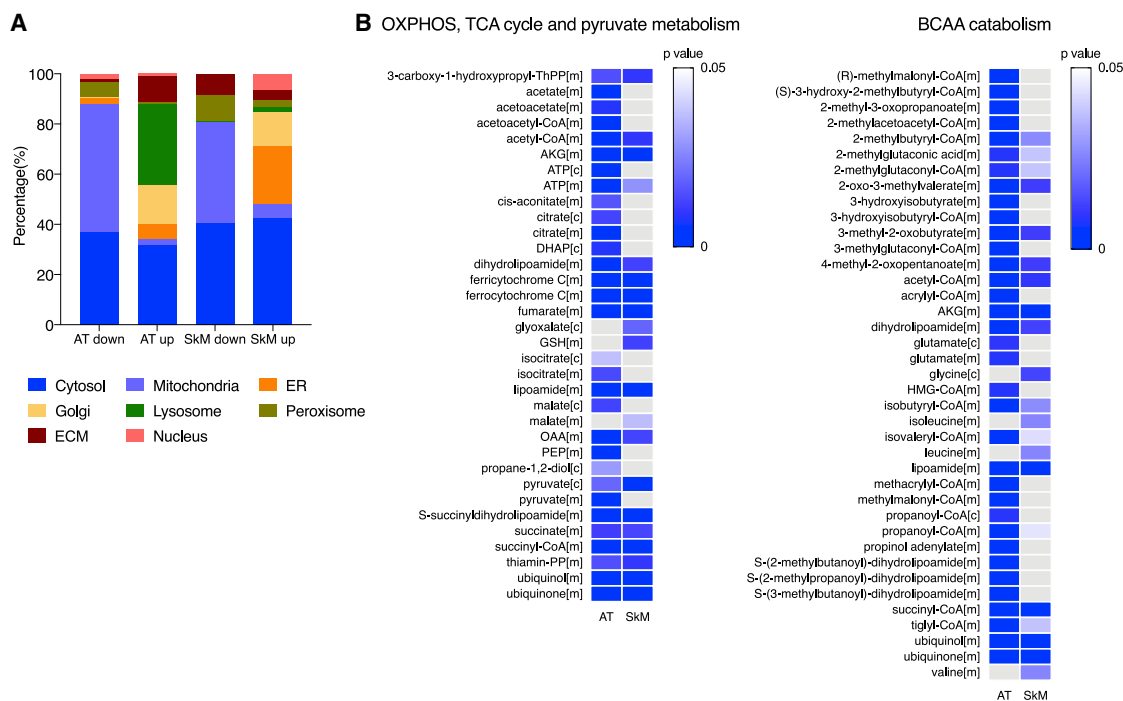
Figure 3. Reporter metabolite representation for heavier co-twins

The reporter metabolites algorithm marks the regions during metabolism around which significant transcriptional changes occur in AT (n = 49 twin pairs) and SkM (n = 44 twin pairs). Reporter metabolites are obtained using the p values calculated from the comparison of heavier co-twins with leaner co-twins. A) Reporter metabolites for the associated subcellular compartments and divided based on the direction (down/up) of the related gene sets (nominal p < 0.05) in the heavier co-twins.

(B) Reporter metabolites associated with key mitochondrion-related pathways were compared between AT and SkM (nominal p < 0.05). The heatmap shows the downregulated gene sets in the heavier co-twins that are significant in at least one of the tissues. In AT, no upregulated gene sets were associated with these pathways. In SkM, the gene set associated with citrate [c] was upregulated (data not shown). ER, endoplasmic reticulum; [c], cytosol; [m], mitochondrion; [p], peroxisome.

associations for multiple measures for adiposity, insulin resistance, LDL, TAG, and CRP in adipose tissue, again observing no associations in skeletal muscle, except for body fat percentage and high-density lipoprotein (HDL) (Figure 5). These results imply that, in acquired obesity, mitochondrial and inflammatory pathways correlate more closely with metabolic health in adipose tissue than in skeletal muscle tissue.

Finally, we studied the relationship between significantly altered metabolites in adipose tissue and skeletal muscle tissue and clinical outcomes among co-twins (Table S6). For adipose tissue, we found that creatine was significantly associated negatively with multiple measures of adiposity, adipocyte size, insulin resistance, and lipid metabolism, whereas the ceramide C18:1Cer was associated positively with measures for adiposity and HDL. For skeletal muscle, pyruvate was significantly positively associated with measures for adiposity and lipid metabolism but not insulin resistance or adipocyte size. Furthermore, skeletal muscle proinflammatory polyunsaturated fatty acid-related eicosanoids were primarily significantly associated positively associated with measures for adiposity but not with other clinical measurements. Last, we associated six previously unexplored lipid-related metabolites that were significantly lower in both tissues in the heavier co-twins, including two oxylipins (Table S6). Overall, these six lipid-related metabolites were asso-

ciated with multiple measures for adiposity and insulin resistance in both tissues, with the exception of the oxylipin 9,12,13-trihydroxyoctadecenoic acid (TriHOME) in adipose tissue.

DISCUSSION

This study describes a global metabolic profile in adipose tissue and skeletal muscle characteristic of acquired obesity. We adopted a novel approach by combining detailed phenotyping from 49 BMI-discordant monozygotic twin pairs with comprehensive collections of adipose and skeletal muscle tissue samples using multiomics and genome-scale metabolic modeling. Our results predominantly reflect environmental and lifestyle factors, given our unique BMI-discordant twin study design. Furthermore, our study provides an opportunity to compare the role of adipose tissue and skeletal muscle in the same individuals in development of obesity-related complications.

Excess body weight was associated with transcriptional downregulation of mitochondrial and nutrient-sensing pathways as well as upregulation of inflammatory pathways in adipose tissue and skeletal muscle in heavier co-twins compared with their leaner co-twins (Figure 6). In skeletal muscle, we observed higher levels of glycolytic proteins and metabolites, including
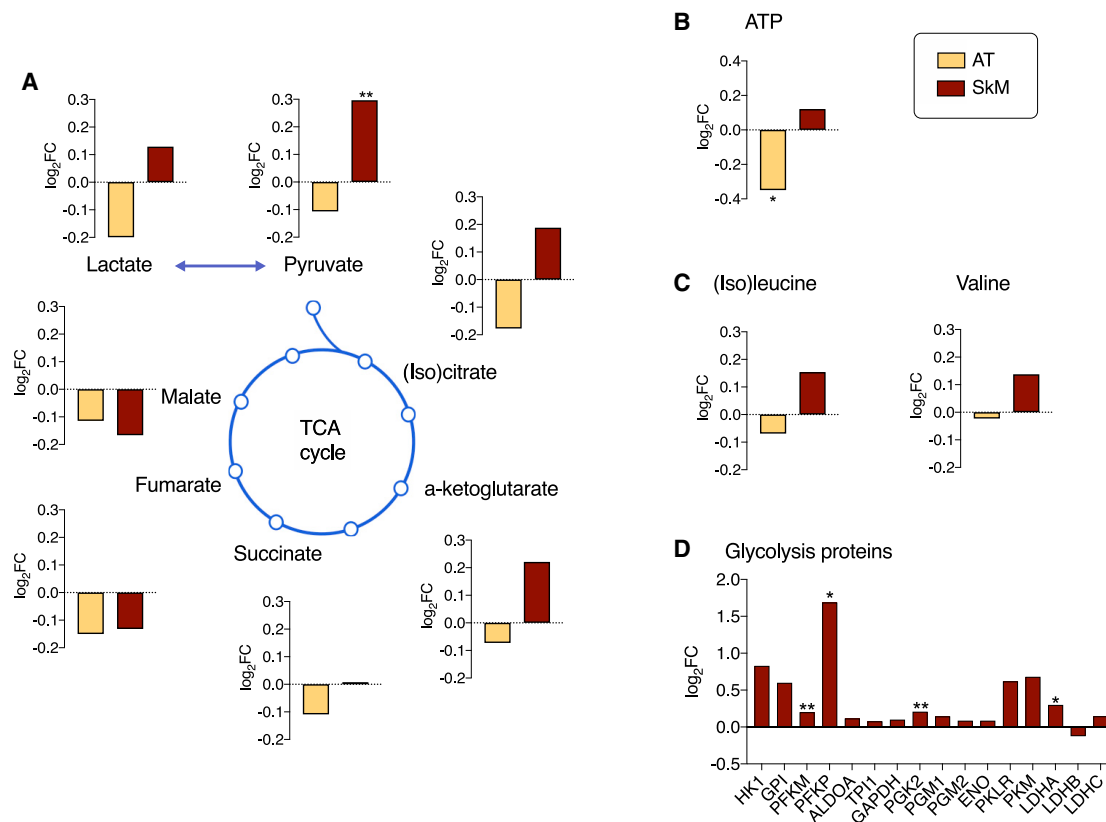
Figure 4. Metabolites and proteins among co-twins in AT and SkM

(A–D) The direction ($\log_2$-fold changes) of the TCA cycle and pyruvate metabolite levels in the heavier co-twins (A), $\log_2$-fold changes of OXPHOS metabolites (B), $\log_2$-fold changes in the BCAA cycle metabolite levels (C), and $\log_2$-fold changes of the glycolysis protein levels in SkM (D). AT (yellow, n = 47 twin pairs); SkM (red, n = 40 twin pairs for metabolomics, n = 48 pairs for proteomics). **nominal $p < 0.01$, *nominal $p < 0.05$.

lactate dehydrogenase and pyruvate, as well as redox stress proteins (Figure 6). In adipose tissue, we found lower creatine levels. Furthermore, in both tissues, we identified higher levels of multiple proinflammatory lipids and lower levels of the same six lipid-related metabolites at the metabolome level. Overall, the effects of surplus body weight appeared to be more pronounced in adipose tissue than in skeletal muscle. Accordingly, in adipose tissue, but not in skeletal muscle tissue, altered mitochondrial and inflammation pathways were associated with a fatty liver, insulin resistance, and dyslipidemia.

One key finding was parallel transcriptional downregulation of mitochondrial oxidative pathways in adipose tissue and skeletal muscle. These pathways were downregulated more in adipose tissue than in skeletal muscle. Because obesity is a significant bioenergetic challenge to the body, it is often associated with mitochondrial oxidative dysregulation. Indeed, lower transcript and protein levels of mitochondria emerged consistently in both tissues in obesity and T2DM using omics platforms.[9–11,24–26,39] However, most studies have focused more on adverse metabolic health aberrations than obesity per se, specifically among skeletal muscle tissue studies. Because adipose tissue is a low-oxygen-consuming tissue,[40] it is slightly counterintuitive that adipose tissue exhibits stronger downregulation of oxidative pathways than

skeletal muscle tissue in obesity. Nevertheless, our results agree with two previous microarray-based studies.[33,34] In those studies, adipose tissue genes were expressed differentially than genes in skeletal muscle tissue in insulin resistance (irrespective of obesity) with downregulated mitochondrial catabolic pathways[33,34] and upregulated inflammation.[33] These findings indicate that adipose tissue is a key metabolic tissue in acquired obesity and that alterations in adipose tissue mitochondria may precede those of skeletal muscle.

In addition to the well-known role of mitochondria in bioenergetics, other vital metabolic functions of mitochondria include generating anabolic precursors for macromolecules, producing metabolic byproducts such as reactive oxygen species (ROS) and lipid intermediates, and using mechanisms to clear or utilize waste products.[41] Our findings related to concomitantly downregulated mitochondrial metabolism and upregulated inflammation in both tissues is intriguing and in line with previous findings in adipose tissue[9–11,33] and skeletal muscle.[42] However, the underlying mechanisms for the two seemingly closely connected biological phenomena remain unclear. Here we propose that "underachieving" mitochondria in acquired obesity give rise to metabolic stress (e.g., increased ROS), accelerating inflammation. Other possible mechanisms include fatty acid and
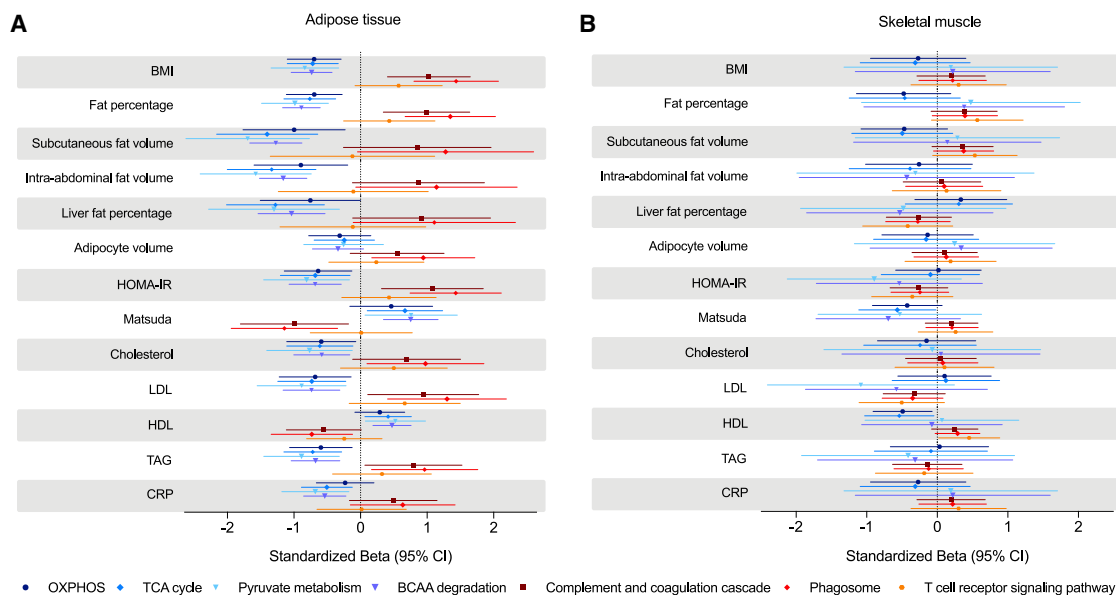
Figure 5. Within-pair associations of four mitochondrial and three inflammatory pathways with clinical outcome measures

(A) Standardized coefficients (βs) in linear mixed models with the delta clinical outcome between co-twins as the dependent variable, the delta for the mitochondrial and inflammatory pathways scores as the fixed effect, and family ID as a random effect and adjusted for sex, age, and diabetes status in AT (n = 49 twin pairs). (B) Standardized coefficients (βs) in linear mixed models with the delta clinical outcomes between co-twins as the dependent variable, the delta for the mitochondrial and inflammatory pathways scores as the fixed effect, and family ID as a random effect and adjusted for sex, age, and diabetes status in SkM (n = 44 twin pairs).

Error bars denote 95% confidence intervals. BMI, body mass index; HDL, high-density lipoprotein; LDL, low-density lipoprotein; TAG, triacylglycerol; HOMA-IR, homeostatic model for the assessment of insulin resistance; CRP, C-reactive protein.

ceramide metabolism regulation and apoptosis by mitochondria,[43] processes we observed to be altered significantly in the heavier co-twins and associated frequently with adipose tissue inflammation.[7] In addition, we observed upregulated lysosomal and Golgi apparatus-related metabolic networks in both tissues, identified similarly as closely related to dysregulated mitochondria and inflammatory processes.[44] Additional studies, however, are needed to provide experimental evidence to support our proposed causal link between mitochondria and obesity-associated inflammation.

In skeletal muscle, our results suggest a shift in fuel partitioning from mitochondrial oxidation to cytosolic glycolysis with preferential use of anaerobic glycolysis under normoxic conditions. Alongside transcriptional mitochondrial oxidative downregulation, we observed higher pyruvate levels in acquired obesity, accompanied by higher glycolytic phosphofructokinases (PFKM and PFKP) and LDHA protein levels. Higher skeletal muscle glycolytic protein levels have been identified in women with morbid obesity.[45] Moreover, downregulated pyruvate uptake into mitochondria has been associated with increased pyruvate and circulating lactate levels in mice,[46] leading to increased whole-body energy expenditure. Another interesting finding may be the pattern of higher TCA metabolites among heavier co-twins up to alpha-ketoglutarate dehydrogenase. This finding resembles glutamine-dependent reductive carboxylation, discovered previously in several mammalian cell lines.[47] In addition, reverse adaptation of the TCA cycle produces citrate and lipids via glutamine-derived alpha-ketoglutarate. However, no

conclusions regarding whether such metabolic routes occur in the skeletal muscle of heavier co-twins can be made based on the current data. Our data suggest an attempt to maintain energetic and metabolic balance in the presence of excessive nutrients in the early stages of obesity.

Interestingly, in adipose tissue, we also observed significantly lower creatine levels in the heavier co-twins, accompanied by the downregulated creatine transporter *SLC6A8*. Along with the classically appreciated energy-buffering role (recycling ATP) in skeletal muscle, recent work indicates that creatine has a pleiotropic role in diverse cell types and physiological conditions.[48] For instance, in rodent brown adipose tissue, creatine appears to closely link to mitochondria by controlling thermogenic respiration, and loss of this metabolite impaired whole-body energy expenditure, leading to obesity.[49] However, the specific function of creatine in human white adipose tissue remains unexamined. In addition, except for *CIDEA*, we did not observe differences in markers of brown/beige adipose tissue (e.g., *UCP1* and *PRDM16*) between co-twins.

We also found that multiple metabolites of polyunsaturated fatty acids were altered in acquired obesity. In skeletal muscle, we detected high eicosanoid levels, known as powerful mediators of inflammation,[50] in the heavier co-twins. In addition, in both tissues, we found lower levels of potentially interesting lipid-related metabolites, including two oxylipins (e.g., polyunsaturated fatty acid derivatives) in the heavier co-twins. Overall, these six lipid-related metabolites were associated with multiple measures of adiposity and insulin resistance in both tissues, with
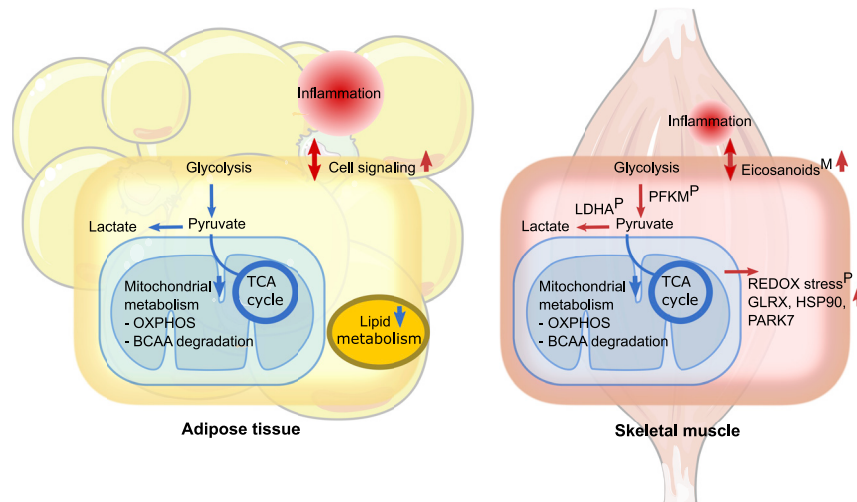
Figure 6. Summary of key metabolic differences in AT and SkM tissue metabolism in acquired obesity

Results from AT (transcriptomics and metabolomics) and SkM (transcriptomics, proteomics, and metabolomics) are included. Significant differences between co-twins from proteomics are indicated by [P] and metabolomics by [M] (nominal p < 0.05). The color of the arrows reflects the differential expressions associated with the heavier co-twins, where blue indicates downregulation, and red indicates upregulation. OXPHOS, oxidative phosphorylation; BCAA, branched-chain amino acids.

the exception of the oxylipin 9,12,13-TriHOME in adipose tissue. The function of these lipids remains unclear. So far, other oxylipins appear to affect tissue differentiation processes,[51] lipid storage,[52] or the process of adipocyte "browning."[53] Experimental studies should follow up on these results.

Finally, the finding that adipose tissue relates more to metabolic health in acquired obesity than skeletal muscle is an important message for prevention of obesity-related complications. In adipose tissue, transcriptional mitochondrial downregulation and inflammation upregulation are associated with a fatty liver, insulin resistance, and dyslipidemia. This indicates that metabolic alterations in adipose tissue function occur during the early stages of the cascade of events, eventually leading to metabolic diseases.[5] Mitochondrial downregulation and upregulated inflammation could accelerate adipose tissue dysfunction, leading to ectopic lipid accumulation in the liver and skeletal muscle with harmful sequelae, such as insulin resistance[6] and non-alcoholic fatty liver disease[8].

The major strength of this work is that our BMI-discordant monozygotic co-twin research design provides an outstanding, well-controlled human study design closely matching genes, age, sex, and the intrauterine and childhood environment between the leaner and heavier groups. Hence, phenotypic differences within a monozygotic twin pair can be attributed to acquired (lifestyle) factors. Our study also uses a systems biology approach in humans covering the transcriptome, proteome, and metabolome in two key metabolic tissue types. This multiomics approach in a well-phenotyped BMI-discordant monozygotic twin model with a large weight discordance (17.1 ± 9.0 kg, 5.8 kg/m^2) allows us to investigate the (patho)physiological responses of surplus body weight on adipose tissue and skeletal muscle, independent of genetic factors.

We show that metabolic alterations in adipose tissue appear to be more pronounced and more related to metabolic health than skeletal muscle in acquired obesity. Furthermore, a key finding is that mitochondrion-related and nutrient-sensing pathways were downregulated in adipose tissue and skeletal muscle in acquired obesity. Concomitantly, we observed simultaneous upregulation of inflammatory pathways, particularly in adipose tissue. We argue that, because of a high nutrition load, adipose tissue and skeletal muscle tissue no longer sufficiently shift between catabolic and anabolic reactions in acquired obesity. Consequently, the cells in these tissues increase their intracellular communication and activate emergency responses such as inflammation. Mitochondria may serve as key sensors of such processes. However, the underlying mechanisms that drive the observed differences in metabolic functions of mitochondria and inflammation in obesity require further study.

Limitations of study

The primary limitation associated with the current study is its cross-sectional nature. Although we can exclude genetic and shared early environmental factors from the observed associations, our cross-sectional design prohibits causal inferences. Furthermore, because the heavier co-twins exhibited poorer metabolic health, some of the findings in our differential expression analyses may arise from obesity-associated metabolic differences between the co-twins. Finally, another limitation of the present study is that, for ethical reasons, we do not have data regarding visceral adipose tissue, which previous studies have found to be strongly associated with metabolic health.[54] Experimental studies should follow up on these findings to fully elucidate the biological mechanisms.

STAR★METHODS

Detailed methods are provided in the online version of this paper and include the following:

- KEY RESOURCES TABLE
- RESOURCE AVAILABILITY
  - Lead contact
  - Materials availability
  - Data and code availability
- EXPERIMENTAL MODEL AND SUBJECT DETAILS
  - Twin participants
- METHOD DETAILS
  - Study protocol
  - Liver fat content
  - Intra-abdominal and subcutaneous fat
  - Clinical chemistry
  - Insulin sensitivity

- ○ Adipose tissue and muscle biopsy collection
- ○ Adipocyte size measurements
- ○ Adipose tissue and muscle transcriptomics
- ○ Skeletal muscle proteomics analysis
- ○ Adipose tissue and muscle metabolomics
- QUANTIFICATION AND STATISTICAL ANALYSIS
  - ○ Statistical analyses
  - ○ Participant characteristics
  - ○ Proteomics and metabolomics data preprocessing
  - ○ Differential expression analysis
  - ○ Biological pathway analyses
  - ○ Genome-scale metabolic models
  - ○ Associations with clinical variables

SUPPLEMENTAL INFORMATION

Supplemental information can be found online at https://doi.org/10.1016/j.xcrm.2021.100226.

AUTHOR CONTRIBUTIONS

S.H., J. Kaprio, A.R., and K.H.P. designed the research and collected the study data. P.P. generated the RNA-seq data, and M. Alvarez, A.K., Z.M., T.T., and P.P. participated in RNA-seq analysis. E.G.W. generated the proteomics data, and N.S. and R.J. participated in proteomics data collection. N.Z. generated the metabolomics data. B.W.v.d.K., S.S., A.L., M. Arif, M.M. and A.O. performed the statistical analyses as follows: B.W.v.d.K. and S.S. analyzed the clinical parameters; M. Arif, M.M., and A.O. performed the transcriptomics, reporter metabolite, and pathway analyses; A.L. performed the proteomics and metabolomics analyses; and M.M. examined the associations between the pathways and metabolites with clinical parameters. A.H., J.L., J. Kuula, P.-H.G., and N.L. participated in imaging of the twins. B.W.v.d.K., S.S., A.L., M. Arif, M.M., S.H., A.M., P.P., and K.H.P. contributed to data interpretation. K.H.P. and A.M. supervised the work. B.W.v.d.K., S.S., and K.H.P. wrote the manuscript. All of the authors revised the content of the manuscript and read and approved the manuscript before submission and publication. K.H.P. is the guarantor of this work and, as such, had full access to all of the data used in this study; she takes responsibility for the integrity of the data and the accuracy of the data analysis.

DECLARATION OF INTERESTS

The authors declare no competing interests.

REFERENCES

1. GBD 2015 Obesity Collaborators; Afshin, A., Forouzanfar, M.H., Reitsma, M.B., Sur, P., Estep, K., Lee, A., Marczak, L., Mokdad, A.H., Moradi-Lakeh, M., et al. (2017). Health Effects of Overweight and Obesity in 195 Countries over 25 Years. N. Engl. J. Med. *377*, 13–27.

2. Blüher, M. (2019). Obesity: global epidemiology and pathogenesis. Nat. Rev. Endocrinol. *15*, 288–298.

3. Longo, M., Zatterale, F., Naderi, J., Parrillo, L., Formisano, P., Raciti, G.A., Beguinot, F., and Miele, C. (2019). Adipose Tissue Dysfunction as Determinant of Obesity-Associated Metabolic Complications. Int. J. Mol. Sci. *20*, 2358.

4. Rutkowski, J.M., Stern, J.H., and Scherer, P.E. (2015). The cell biology of fat expansion. J. Cell Biol. *208*, 501–512.

5. Heinonen, S., Jokinen, R., Rissanen, A., and Pietiläinen, K.H. (2020). White adipose tissue mitochondrial metabolism in health and in obesity. Obes. Rev. *21*, e12958.

6. Stinkens, R., Goossens, G.H., Jocken, J.W.E., and Blaak, E.E. (2015). Targeting fatty acid metabolism to improve glucose metabolism. Obes. Rev. *16*, 715–757.

7. Reilly, S.M., and Saltiel, A.R. (2017). Adapting to obesity with adipose tissue inflammation. Nat. Rev. Endocrinol. *13*, 633–643.

8. Yki-Järvinen, H. (2014). Non-alcoholic fatty liver disease as a cause and a consequence of metabolic syndrome. Lancet Diabetes Endocrinol. *2*, 901–910.

9. Muniandy, M., Heinonen, S., Yki-Järvinen, H., Hakkarainen, A., Lundbom, J., Lundbom, N., Kaprio, J., Rissanen, A., Ollikainen, M., and Pietiläinen, K.H. (2017). Gene expression profile of subcutaneous adipose tissue in BMI-discordant monozygotic twin pairs unravels molecular and clinical changes associated with sub-types of obesity. Int. J. Obes. *41*, 1176–1184.

10. Pietiläinen, K.H., Naukkarinen, J., Rissanen, A., Saharinen, J., Ellonen, P., Keränen, H., Suomalainen, A., Götz, A., Suortti, T., Yki-Järvinen, H., et al. (2008). Global transcript profiles of fat in monozygotic twins discordant for BMI: pathways behind acquired obesity. PLoS Med. *5*, e51.

11. Soronen, J., Laurila, P.-P., Naukkarinen, J., Surakka, I., Ripatti, S., Jauhiainen, M., Olkkonen, V.M., and Yki-Järvinen, H. (2012). Adipose tissue gene expression analysis reveals changes in inflammatory, mitochondrial respiratory and lipid metabolic pathways in obese insulin-resistant subjects. BMC Med. Genomics *5*, 9.

12. Das, S.K., Ma, L., and Sharma, N.K. (2015). Adipose tissue gene expression and metabolic health of obese adults. Int. J. Obes. *39*, 869–873.

13. van der Kolk, B.W., Kalafati, M., Adriaens, M., van Greevenbroek, M.M.J., Vogelzangs, N., Saris, W.H.M., Astrup, A., Valsesia, A., Langin, D., van der Kallen, C.J.H., et al. (2019). Subcutaneous Adipose Tissue and Systemic Inflammation Are Associated With Peripheral but Not Hepatic Insulin Resistance in Humans. Diabetes *68*, 2247–2258.

14. Rydén, M., Hrydziuszko, O., Mileti, E., Raman, A., Bornholdt, J., Boyd, M., Toft, E., Qvist, V., Näslund, E., Thorell, A., et al. (2016). The Adipose Transcriptional Response to Insulin Is Determined by Obesity, Not Insulin Sensitivity. Cell Rep. *16*, 2317–2326.

15. Wiklund, P., Zhang, X., Pekkala, S., Autio, R., Kong, L., Yang, Y., Keinänen-Kiukaanniemi, S., Alen, M., and Cheng, S. (2016). Insulin resistance is associated with altered amino acid metabolism and adipose tissue dysfunction in normoglycemic women. Sci. Rep. *6*, 24540.

16. Heinonen, S., Saarinen, L., Naukkarinen, J., Rodríguez, A., Frühbeck, G., Hakkarainen, A., Lundbom, J., Lundbom, N., Vuoltenaho, K., Moilanen, E., et al. (2014). Adipocyte morphology and implications for metabolic derangements in acquired obesity. Int. J. Obes. *38*, 1423–1431.

17. Yin, Z., Deng, T., Peterson, L.E., Yu, R., Lin, J., Hamilton, D.J., Reardon, P.R., Sherman, V., Winnier, G.E., Zhan, M., et al. (2014). Transcriptome analysis of human adipocytes implicates the NOD-like receptor pathway in obesity-induced adipose inflammation. Mol. Cell. Endocrinol. *394*, 80–87.

18. Kulytė, A., Ehrlund, A., Arner, P., and Dahlman, I. (2017). Global transcriptome profiling identifies KLF15 and SLC25A10 as modifiers of adipocytes insulin sensitivity in obese women. PLoS ONE *12*, e0178485.

19. Mastrangelo, A., Panadero, M.I., Pérez, L.M., Gálvez, B.G., García, A., Barbas, C., and Rupérez, F.J. (2016). New insight on obesity and adipose-derived stem cells using comprehensive metabolomics. Biochem. J. *473*, 2187–2203.

20. Wu, C., Xu, G., Tsai, S.A., Freed, W.J., and Lee, C.T. (2017). Transcriptional profiles of type 2 diabetes in human skeletal muscle reveal insulin resistance, metabolic defects, apoptosis, and molecular signatures of immune activation in response to infections. Biochem. Biophys. Res. Commun. *482*, 282–288.

21. Scott, L.J., Erdos, M.R., Huyghe, J.R., Welch, R.P., Beck, A.T., Wolford, B.N., Chines, P.S., Didion, J.P., Narisu, N., Stringham, H.M., et al. (2016). The genetic regulatory signature of type 2 diabetes in human skeletal muscle. Nat. Commun. *7*, 11764.

22. Väremo, L., Henriksen, T.I., Scheele, C., Broholm, C., Pedersen, M., Uhlén, M., Pedersen, B.K., and Nielsen, J. (2017). Type 2 diabetes and obesity induce similar transcriptional reprogramming in human myocytes. Genome Med. *9*, 47.

23. Chae, S., Kim, S.-J., Do Koo, Y., Lee, J.H., Kim, H., Ahn, B.Y., Ha, Y.C., Kim, Y.H., Jang, M.G., Koo, K.H., et al. (2018). A mitochondrial proteome profile indicative of type 2 diabetes mellitus in skeletal muscles. Exp. Mol. Med. *50*, 1–14.

24. Formentini, L., Ryan, A.J., Gálvez-Santisteban, M., Carter, L., Taub, P., Lapek, J.D., Jr., Gonzalez, D.J., Villarreal, F., Ciaraldi, T.P., Cuezva, J.M., and Henry, R.R. (2017). Mitochondrial H⁺-ATP synthase in human skeletal muscle: contribution to dyslipidaemia and insulin resistance. Diabetologia *60*, 2052–2065.

25. Giebelstein, J., Poschmann, G., Højlund, K., Schechinger, W., Dietrich, J.W., Levin, K., Beck-Nielsen, H., Podwojski, K., Stühler, K., Meyer, H.E., and Klein, H.H. (2012). The proteomic signature of insulin-resistant human skeletal muscle reveals increased glycolytic and decreased mitochondrial enzymes. Diabetologia *55*, 1114–1127.

26. Hwang, H., Bowen, B.P., Lefort, N., Flynn, C.R., De Filippis, E.A., Roberts, C., Smoke, C.C., Meyer, C., Højlund, K., Yi, Z., and Mandarino, L.J. (2010). Proteomics analysis of human skeletal muscle reveals novel abnormalities in obesity and type 2 diabetes. Diabetes *59*, 33–42.

27. Campbell, L.E., Langlais, P.R., Day, S.E., Coletta, R.L., Benjamin, T.R., De Filippis, E.A., Madura, J.A., 2nd, Mandarino, L.J., Roust, L.R., and Coletta, D.K. (2016). Identification of Novel Changes in Human Skeletal Muscle Proteome After Roux-en-Y Gastric Bypass Surgery. Diabetes *65*, 2724–2731.

28. Baker, P.R., 2nd, Boyle, K.E., Koves, T.R., Ilkayeva, O.R., Muoio, D.M., Houmard, J.A., and Friedman, J.E. (2015). Metabolomic analysis reveals altered skeletal muscle amino acid and fatty acid handling in obese humans. Obesity (Silver Spring) *23*, 981–988.

29. Hernández-Alvarez, M.I., Díaz-Ramos, A., Berdasco, M., Cobb, J., Planet, E., Cooper, D., Pazderska, A., Wanic, K., O'Hanlon, D., Gomez, A., et al. (2017). Early-onset and classical forms of type 2 diabetes show impaired expression of genes involved in muscle branched-chain amino acids metabolism. Sci. Rep. *7*, 13850.

30. Kogelman, L.J.A., Fu, J., Franke, L., Greve, J.W., Hofker, M., Rensen, S.S., and Kadarmideen, H.N. (2016). Inter-Tissue Gene Co-Expression Networks between Metabolically Healthy and Unhealthy Obese Individuals. PLoS ONE *11*, e0167519.

31. Stentz, F.B., and Kitabchi, A.E. (2007). Transcriptome and proteome expressions involved in insulin resistance in muscle and activated T-lymphocytes of patients with type 2 diabetes. Genomics Proteomics Bioinformatics *5*, 216–235.

32. Calimlioglu, B., Karagoz, K., Sevimoglu, T., Kilic, E., Gov, E., and Arga, K.Y. (2015). Tissue-Specific Molecular Biomarker Signatures of Type 2 Diabetes: An Integrative Analysis of Transcriptomics and Protein-Protein Interaction Data. OMICS *19*, 563–573.

33. Elbein, S.C., Kern, P.A., Rasouli, N., Yao-Borengasser, A., Sharma, N.K., and Das, S.K. (2011). Global gene expression profiles of subcutaneous adipose and muscle from glucose-tolerant, insulin-sensitive, and insulin-resistant individuals matched for BMI. Diabetes *60*, 1019–1029.

34. Sharma, N.K., Sajuthi, S.P., Chou, J.W., Calles-Escandon, J., Demons, J., Rogers, S., Ma, L., Palmer, N.D., McWilliams, D.R., Beal, J., et al. (2016). Tissue-Specific and Genetic Regulation of Insulin Sensitivity-Associated Transcripts in African Americans. J. Clin. Endocrinol. Metab. *101*, 1455–1468.

35. Kučera, J., Spáčil, Z., Friedecký, D., Novák, J., Pekař, M., and Bienertová-Vašků, J. (2018). Human White Adipose Tissue Metabolome: Current Perspective. Obesity (Silver Spring) *26*, 1870–1878.

36. Kaprio, J., Bollepalli, S., Buchwald, J., Iso-Markku, P., Korhonen, T., Kovanen, V., Kujala, U., Laakkonen, E.K., Latvala, A., Leskinen, T., et al. (2019). The Older Finnish Twin Cohort - 45 Years of Follow-up. Twin Res. Hum. Genet. *22*, 240–254.

37. Stefan, D., Di Cesare, F., Andrasescu, A., Popa, E., Lazariev, A., Vescovo, E., Strbak, O., Williams, S., Starcuk, Z., and Cabanas, M. (2009). Quantitation of magnetic resonance spectroscopy signals: the jMRUI software package. Meas. Sci. Technol. *20*, 104035.

38. Robinson, J.L., Kocabaş, P., Wang, H., Cholley, P.E., Cook, D., Nilsson, A., Anton, M., Ferreira, R., Domenzain, I., Billa, V., et al. (2020). An atlas of human metabolism. Sci. Signal. *13*, eaaz1482.

39. Heinonen, S., Buzkova, J., Muniandy, M., Kaksonen, R., Ollikainen, M., Ismail, K., Hakkarainen, A., Lundbom, J., Lundbom, N., Vuolteenaho, K., et al. (2015). Impaired Mitochondrial Biogenesis in Adipose Tissue in Acquired Obesity. Diabetes *64*, 3135–3145.

40. Lempesis, I.G., van Meijel, R.L.J., Manolopoulos, K.N., and Goossens, G.H. (2020). Oxygenation of adipose tissue: A human perspective. Acta Physiol. (Oxf.) *228*, e13298–e17.

41. Spinelli, J.B., and Haigis, M.C. (2018). The multifaceted contributions of mitochondria to cellular metabolism. Nat. Cell Biol. *20*, 745–754.

42. Wu, H., and Ballantyne, C.M. (2017). Skeletal muscle inflammation and insulin resistance in obesity. J. Clin. Invest. *127*, 43–54.

43. Bock, F.J., and Tait, S.W.G. (2020). Mitochondria as multifaceted regulators of cell death. Nat. Rev. Mol. Cell Biol. *21*, 85–100.

44. Todkar, K., Ilamathi, H.S., and Germain, M. (2017). Mitochondria and Lysosomes: Discovering Bonds. Front. Cell Dev. Biol. *5*, 106.

45. Hittel, D.S., Hathout, Y., Hoffman, E.P., and Houmard, J.A. (2005). Proteome analysis of skeletal muscle from obese and morbidly obese women. Diabetes *54*, 1283–1288.

46. Sharma, A., Oonthonpan, L., Sheldon, R.D., Rauckhorst, A.J., Zhu, Z., Tompkins, S.C., Cho, K., Grzesik, W.J., Gray, L.R., Scerbo, D.A., et al. (2019). Impaired skeletal muscle mitochondrial pyruvate uptake rewires glucose metabolism to drive whole-body leanness. eLife *8*, 485.

47. Mullen, A.R., Wheaton, W.W., Jin, E.S., Chen, P.H., Sullivan, L.B., Cheng, T., Yang, Y., Linehan, W.M., Chandel, N.S., and DeBerardinis, R.J. (2011). Reductive carboxylation supports growth in tumour cells with defective mitochondria. Nature *481*, 385–388.

48. Kazak, L., and Cohen, P. (2020). Creatine metabolism: energy homeostasis, immunity and cancer biology. Nat. Rev. Endocrinol. *16*, 421–436.

49. Kazak, L., Chouchani, E.T., Lu, G.Z., Jedrychowski, M.P., Bare, C.J., Mina, A.I., Kumari, M., Zhang, S., Vuckovic, I., Laznik-Bogoslavski, D., et al. (2017). Genetic Depletion of Adipocyte Creatine Metabolism Inhibits Diet-Induced Thermogenesis and Drives Obesity. Cell Metab. *26*, 693.

50. Korotkova, M., and Lundberg, I.E. (2014). The skeletal muscle arachidonic acid cascade in health and inflammatory disease. Nat. Rev. Rheumatol. *10*, 295–303.

51. Madsen, L., Petersen, R.K., Sørensen, M.B., Jørgensen, C., Hallenborg, P., Pridal, L., Fleckner, J., Amri, E.Z., Krieg, P., Furstenberger, G., et al. (2003). Adipocyte differentiation of 3T3-L1 preadipocytes is dependent on lipoxygenase activity during the initial stages of the differentiation process. Biochem. J. *375*, 539–549.

52. Zahradka, P., Neumann, S., Aukema, H.M., and Taylor, C.G. (2017). Adipocyte lipid storage and adipokine production are modulated by lipoxygenase-derived oxylipins generated from 18-carbon fatty acids. Int. J. Biochem. Cell Biol. *88*, 23–30.

53. Dieckmann, S., Maurer, S., Fromme, T., Colson, C., Virtanen, K.A., Amri, E.Z., and Klingenspor, M. (2020). Fatty Acid Metabolite Profiling Reveals Oxylipins as Markers of Brown but Not Brite Adipose Tissue. Front. Endocrinol. (Lausanne) *11*, 73.

54. Klöting, N., and Blüher, M. (2014). Adipocyte dysfunction, inflammation and metabolic syndrome. Rev. Endocr. Metab. Disord. *15*, 277–287.

55. Wishart, D.S., Jewison, T., Guo, A.C., Wilson, M., Knox, C., Liu, Y., Djoumbou, Y., Mandal, R., Aziat, F., Dong, E., et al. (2013). HMDB 3.0–The Human Metabolome Database in 2013. Nucleic Acids Res. *41*, D801–D807.

56. Rosenberger, G., Koh, C.C., Guo, T., Röst, H.L., Kouvonen, P., Collins, B.C., Heusel, M., Liu, Y., Caron, E., Vichalkovski, A., et al. (2014). A repository of assays to quantify 10,000 human proteins by SWATH-MS. Sci. Data *1*, 140031.

57. Dobin, A., Davis, C.A., Schlesinger, F., Drenkow, J., Zaleski, C., Jha, S., Batut, P., Chaisson, M., and Gingeras, T.R. (2013). STAR: ultrafast universal RNA-seq aligner. Bioinformatics *29*, 15–21.

58. Jun, G., Flickinger, M., Hetrick, K.N., Romm, J.M., Doheny, K.F., Abecasis, G.R., Boehnke, M., and Kang, H.M. (2012). Detecting and estimating contamination of human DNA samples in sequencing and array-based genotype data. Am. J. Hum. Genet. *91*, 839–848.

59. Anders, S., Pyl, P.T., and Huber, W. (2015). HTSeq–a Python framework to work with high-throughput sequencing data. Bioinformatics *31*, 166–169.

60. Ritchie, M.E., Phipson, B., Wu, D., Hu, Y., Law, C.W., Shi, W., and Smyth, G.K. (2015). limma powers differential expression analyses for RNA-sequencing and microarray studies. Nucleic Acids Res. *43*, e47.

61. Väremo, L., Nielsen, J., and Nookaew, I. (2013). Enriching the gene set analysis of genome-wide data by incorporating directionality of gene expression and combining statistical hypotheses and methods. Nucleic Acids Res. *41*, 4378–4391.

62. Kuleshov, M.V., Jones, M.R., Rouillard, A.D., Fernandez, N.F., Duan, Q., Wang, Z., Koplev, S., Jenkins, S.L., Jagodnik, K.M., Lachmann, A., et al. (2016). Enrichr: a comprehensive gene set enrichment analysis web server 2016 update. Nucleic Acids Res. *44* (*W1*), W90-7.

63. Mardinoglu, A., Agren, R., Kampf, C., Asplund, A., Nookaew, I., Jacobson, P., Walley, A.J., Froguel, P., Carlsson, L.M., Uhlen, M., and Nielsen, J. (2013). Integration of clinical data with a genome-scale metabolic model of the human adipocyte. Mol. Syst. Biol. *9*, 649.

64. Väremo, L., Scheele, C., Broholm, C., Mardinoglu, A., Kampf, C., Asplund, A., Nookaew, I., Uhlén, M., Pedersen, B.K., and Nielsen, J. (2015). Proteome- and transcriptome-driven reconstruction of the human myocyte metabolic network and its use for identification of markers for diabetes. Cell Rep. *11*, 921–933.

65. Chambers, M.C., Maclean, B., Burke, R., Amodei, D., Ruderman, D.L., Neumann, S., Gatto, L., Fischer, B., Pratt, B., Egertson, J., et al. (2012). A cross-platform toolkit for mass spectrometry and proteomics. Nat. Biotechnol. *30*, 918–920.

66. Teo, G., Kim, S., Tsou, C.-C., Collins, B., Gingras, A.C., Nesvizhskii, A.I., and Choi, H. (2015). mapDIA: Preprocessing and statistical analysis of quantitative proteomics data from data independent acquisition mass spectrometry. J. Proteomics *129*, 108–120.

67. Vanhamme, L., van den Boogaart, A., and Van Huffel, S. (1997). Improved method for accurate and efficient quantification of MRS data with use of prior knowledge. J. Magn. Reson. *129*, 35–43.

68. Kaidesoja, M., Aaltonen, S., Bogl, L.H., Heikkilä, K., Kaartinen, S., Kujala, U.M., Kärkkäinen, U., Masip, G., Mustelin, L., Palviainen, T., et al. (2019). FinnTwin16: A Longitudinal Study from Age 16 of a Population-Based Finnish Twin Cohort. Twin Res. Hum. Genet. *22*, 530–539.

69. Rose, R.J., Salvatore, J.E., Aaltonen, S., Barr, P.B., Bogl, L.H., Byers, H.A., Heikkilä, K., Korhonen, T., Latvala, A., Palviainen, T., et al. (2019). FinnTwin12 Cohort: An Updated Review. Twin Res. Hum. Genet. *22*, 302–311.

70. Baecke, J.A., Burema, J., and Frijters, J.E. (1982). A short questionnaire for the measurement of habitual physical activity in epidemiological studies. Am. J. Clin. Nutr. *36*, 936–942.

71. Kotronen, A., Peltonen, M., Hakkarainen, A., Sevastianova, K., Bergholm, R., Johansson, L.M., Lundbom, N., Rissanen, A., Ridderstråle, M., Groop, L., et al. (2009). Prediction of non-alcoholic fatty liver disease and liver fat using metabolic and genetic factors. Gastroenterology *137*, 865–872.

72. Matsuda, M., and DeFronzo, R.A. (1999). Insulin sensitivity indices obtained from oral glucose tolerance testing: comparison with the euglycemic insulin clamp. Diabetes Care *22*, 1462–1470.

73. Bergström, J., Hermansen, L., Hultman, E., and Saltin, B. (1967). Diet, muscle glycogen and physical performance. Acta Physiol. Scand. *71*, 140–150.

74. Broad Institute (2019). Picard Toolkit. (Broad Institute, GitHub Repository). http://broadinstitute.github.io/picard/.

75. Wu, Y., Williams, E.G., and Aebersold, R. (2017). Application of SWATH Proteomics to Mouse Biology. Curr. Protoc. Mouse Biol. *7*, 130–143.

76. Gillet, L.C., Navarro, P., Tate, S., Röst, H., Selevsek, N., Reiter, L., Bonner, R., and Aebersold, R. (2012). Targeted data extraction of the MS/MS spectra generated by data-independent acquisition: a new concept for consistent and accurate proteome analysis. Mol. Cell Proteomics *11*, O111.016717.

77. Röst, H.L., Rosenberger, G., Navarro, P., Gillet, L., Miladinović, S.M., Schubert, O.T., Wolski, W., Collins, B.C., Malmström, J., Malmström, L., and Aebersold, R. (2014). OpenSWATH enables automated, targeted analysis of data-independent acquisition MS data. Nat. Biotechnol. *32*, 219–223.

78. Ludwig, C., Gillet, L., Rosenberger, G., Amon, S., Collins, B.C., and Aebersold, R. (2018). Data-independent acquisition-based SWATH-MS for quantitative proteomics: a tutorial. Mol. Syst. Biol. *14*, e8126.

79. Fuhrer, T., Heer, D., Begemann, B., and Zamboni, N. (2011). High-throughput, accurate mass metabolome profiling of cellular extracts by flow injection-time-of-flight mass spectrometry. Anal. Chem. *83*, 7074–7080.

80. Chong, J., Wishart, D.S., and Xia, J. (2019). Using MetaboAnalyst 4.0 for Comprehensive and Integrative Metabolomics Data Analysis. Curr. Protoc. Bioinformatics *68*, e86.

STAR★METHODS

KEY RESOURCES TABLE

REAGENT or RESOURCE	SOURCE	IDENTIFIER
Biological samples		
Human blood and tissue samples	This study	N/A
Chemicals, peptides, and recombinant proteins		
DNase I	QIAGEN	Cat No./ID: 79254
Critical commercial assays		
AllPrep RNA, DNA, miRNA Universal Kit	QIAGEN	Cat No./ID: 80224
Deposited data		
RNaseq data	This study	THLBB2021_001
HMDB v3.0 database	Wishart et al. 2013[55]	RRID:SCR_007712
PanHuman library	Rosenberger et al.[56]	http://proteomecentral.proteomexchange.org/cgi/GetDataset?ID=PXD000954
Human reference genome NCBI build 38, GRCh38	Genome Reference Consortium	https://www.ncbi.nlm.nih.gov/projects/genome/assembly/grc/human/
Software and algorithms		
Bioanalyzer 2100 expert software	Agilent	RRID:SCR_018043
STAR v2.5.2b	Dobin et al., 2013[57]	RRID:SCR_015899
Picard	Broad Institute	RRID:SCR_006525
VerifyBamID	Jun et al.[58]	https://github.com/Griffan/VerifyBamID
HTSeq v0.6.1p	Anders et al.[59]	RRID:SCR_005514
limma	Ritchie et al.[60]	RRID:SCR_010943
PIANO	Väremo et al.[61]	RRID:SCR_003200
EnrichR	Kuleshov et al.[62]	RRID:SCR_001575
STRING v11.0	STRING consortium	RRID:SCR_005223
Human Metabolic Atlas	Robinson et al.[38]	https://www.metabolicatlas.org/
iAdipocyte1809	Mardinoglu et al.[63]	https://www.metabolicatlas.org/gems/repository
iMyocyte2419	Väremo et al.[64]	https://www.metabolicatlas.org/gems/repository
OpenSWATH v2.1	Aebersold Group at IMSB, ETH Zurich, University of Toronto and Columbia University	http://openswath.org/en/latest/
Proteowizard 3.0.5533	Chambers et al.[65]	RRID:SCR_012056
Jumbo PyProphet v1.0	Röst lab	http://openswath.org/en/latest/docs/pyprophet_legacy.html
TRIC (in the msproteomicstools 0.8.0 package)	Röst lab	http://msproteomicstools.roestlab.org/
mapDIA v3.0.2	Teo et al.[66]	https://sourceforge.net/projects/mapdia/
jMRUI 6.0 software	Stefan et al.[37]	http://www.jmrui.eu/
AMARES algorithm	Vanhamme et al.[67]	https://www.esat.kuleuven.be/sista/yearreport96/node2.html
ImageJ	NIH	RRID:SCR_003070
ImageJ adipocyte diameter algorithm	Sakari Jukarainen	https://github.com/birgittavdkolk/vanderkolk_etal_2021
GraphPad Prism V8 for Mac	GraphPad software	RRID:SCR_002798
SPSS v24.0 for Mac	IBM	RRID:SCR_019096
R statistical programming language (version 3.3.3)	The R-project	RRID:SCR_001905
Servier Medical Art	Servier	https://smart.servier.com/

RESOURCE AVAILABILITY

Lead contact
Further information and requests for data should be directed to and will be fulfilled by the Lead Contact, Dr. Kirsi H. Pietiläinen (kirsi.pietilainen@helsinki.fi).

Materials availability
This study did not generate new unique reagents.

Data and code availability
RNA sequencing data are part of the 'Twin Study' and are deposited with the Biobank of the Finnish Institute for Health and Welfare (https://thl.fi/en/web/thl-biobank/for-researchers/sample-collections/twin-study) with the identification number THLBB2021_001. For details on accessing the data, see https://thl.fi/en/web/thl-biobank/for-researchers/application-process. All bona fide researchers can apply for the data. The ImageJ macro used for measuring adipocyte diameters can be found at https://github.com/birgittavdkolk/vanderkolk_etal_2021.

EXPERIMENTAL MODEL AND SUBJECT DETAILS

Twin participants
The twin pairs included in this study were recruited from population-based longitudinal studies, FinnTwin16 (n = 2839 pairs[68]) and FinnTwin12 (n = 2578 pairs[69]), as well as the Older Finnish Twin Cohort (n = 2932 pairs[36]), based on their responses to questions regarding weight and height.

Here, we included 49 monozygotic twin pairs discordant for BMI (within-pair difference, ΔBMI $\geq$ 2.5 kg/m^2), from two age groups (27–42 years old and 57–69 years old) and for whom adipose tissue and skeletal muscle multiomics data were available. Twenty-seven pairs were female. Eight pairs were discordant and four pairs were concordant for T2DM, while other pairs reported no T2DM.

The Ethics Committee of the Hospital District of Helsinki and Uusimaa approved the studies and all participants provided their written informed consent. The studies adhered to the principles of the Declaration of Helsinki.

METHOD DETAILS

Study protocol
Participants arrived at the clinical research center the day before the studies. All participants were instructed by a nutritionist to consume an isocaloric diet and to avoid strenuous exercise and alcohol consumption for two days prior to admission. Weight and height were measured after a 12-h overnight fast in light clothing. Body composition was measured using dual-energy X-ray absorptiometry (software version 8.8; DEXA, Lunar Prodigy, Madison, WI, USA), subcutaneous and visceral adipose tissue volumes using magnetic resonance imaging (MRI) and liver fat content using magnetic resonance spectroscopy (MRS). Physical activity was measured using the Baecke questionnaire[70].

Liver fat content
MRI and MRS experiments were performed on a 1.5 Tesla clinical imager (Avanto/Avanto^{fit}, Siemens, Erlangen, Germany). To determine the liver fat content, a 25 × 25 × 25 mm^3 voxel was placed in the middle of the right liver lobe and liver spectra with an echo time (TE) of 30 ms, collecting 4 averages. A point-resolved spectroscopy (PRESS) sequence was used for spatial localization, while signal acquisition was triggered to end exhalation using a navigator belt to eliminate motion artifacts due to respiratory motion, maintained at TR > 4000 ms. Liver spectra were analyzed with the jMRUI 6.0 software[37] and the intensities of methylene and water resonances were determined using the AMARES algorithm.[67] Signal intensities were corrected for the relaxation effects and the liver fat was calculated as an intensity ratio of methylene/(methylene+water). Ratios were further converted to mass fractions as described previously.[71] All spectra were analyzed by a physicist blinded to the clinical data.

Intra-abdominal and subcutaneous fat
MRIs were recorded using the body coil as the transmitter and receiver. A stack of abdominal T1-weighted MRIs (16 slices, slice thickness 10 mm, TR of 91 ms, TE of 5.2 ms and a flip angle of 80°) were obtained from 8 cm above to 8 cm below the L4/5 lumbar intervertebral disks using frequency-selective fat excitation. Areas of visceral and subcutaneous adipose tissue depots were determined from each slice using SliceOmatic (TomoVision, Quebec, Canada) version 5.0 segmentation software using the region-growing routine.

Clinical chemistry
Blood samples were collected following an overnight fast. Whole blood, separated plasma and serum samples were frozen at −80°C until further analysis. Samples were analyzed at the HUSLAB facilities using standardized methods. Concentrations of plasma

glucose were measured using the spectrophotometric hexokinase and glucose-6-phosphate dehydrogenase assay (Gluko-quant glucose/hexokinase, Roche Diagnostics, Basel, Switzerland) with a Hitachi Modular automatic analyzer and serum insulin with a time-resolved immunofluorometric assay (Perkin Elmer, Waltham, MA, USA). Fasting plasma total cholesterol, high-density lipoprotein cholesterol (HDL) and triglyceride concentrations were determined using enzymatic methods (Roche Diagnostics Hitachi, Hitachi Ltd, Tokyo, Japan). Low-density lipoprotein (LDL) cholesterol was calculated using the Friedewald formula. Serum high-sensitivity C-reactive protein (hs-CRP) was measured using the particle-enhanced immunoturbidimetric assay (Cobas CRP (Latex) HS, Roche Diagnostics) on a Modular automatic analyzer (Hitachi Ltd, Tokyo, Japan).

Insulin sensitivity

Participants underwent a standard 4-point oral glucose tolerance test (OGTT). After an overnight fast, venous blood was sampled before (t0) and after a 75-g glucose load was ingested. Blood samples were taken at the HUSLAB facilities at t0, t30, t60 and t120 min to determine glucose and insulin concentrations. The homeostatic model assessment–insulin resistance index was calculated as (fasting glucose (mmol l^{-1}) × fasting insulin (mU l^{-1})/22.5). The Matsuda Index (ISI-M) = 10 000/(G_0 × I_0 × G_{mean} × I_{mean})$^{1/2}$, where G and I represents plasma glucose [mmol dl^{-1}] and insulin [mU l^{-1}] concentrations, respectively, and '0' and 'mean' indicate the fasting value and mean value during OGTT, respectively.[72]

Adipose tissue and muscle biopsy collection

All biopsy collections took place during the fasting (12 h) state following collection of the fasting blood samples. The adipose tissue and skeletal muscle biopsies were taken in sterile conditions under local anesthesia (lidocaine). The subcutaneous adipose tissue biopsies were taken from superficial abdominal adipose tissue near the umbilicus using a surgical technique or through a needle biopsy. A needle muscle biopsy was taken from the vastus lateralis muscle. An incision was made through the skin, after which the sample was taken using a 5-mm Bergström needle.[73] Both tissue specimens were immediately snap-frozen in liquid nitrogen and stored in liquid nitrogen until further analysis.

Adipocyte size measurements

For part of the fresh subcutaneous adipose tissue biopsies, a collagenase digestion was performed. The subcutaneous adipose tissue was minced and incubated for 1 h at 37°C through constant shaking in 10 mL of an adipocyte medium (DMEM/F-12 (1:1) (Invitrogen, Paisley, UK) supplemented with 16-µmol l^{-1} biotin, 18-µmol l^{-1} panthotenate, 100-µmol l^{-1} ascorbate and antibiotic-antimycotic (Invitrogen)), supplemented with 2% bovine serum albumin (Sigma, St Louis, MO, USA) and with 2-mg ml^{-1} collagenase A (Roche, Basel, Switzerland). Digestion was stopped when the adipocyte medium supplemented with 10% newborn calf serum (Sigma) was added, and centrifuged for 10 min at 600 g. After washing the adipocytes with an adipocyte medium, photographs of the adipocytes were then taken using a light microscope (Zeiss, Axioplan2) at x50 magnification. Adipocyte diameters were automatically measured from the images using a custom algorithm for ImageJ (ImageJ 1.42q/ Java 1. 6.0 10 32-bit; https://github.com/birgittavdkolk/vanderkolk_etal_2021), which preprocessed the image to enhance the borders of the adipocytes and then used a circle-detection algorithm to identify the cells. The algorithm was tuned to identify the adipocytes taken using the standardized microscope settings, and validated against 2000 manually measured diameters from 20 pictures (r = 0.85, p < 0.001). Mean adipocyte volume was calculated for each individual using the following formula: $V = \left(\sum_1^{100} \left(\frac{\pi \cdot d_i^3}{6} \right) /100 \right)$. V = cell volume (µm^3), d = cell diameter (µm). Adipocytes were assumed to be spheres.

Adipose tissue and muscle transcriptomics

For total RNA extraction, we used ~250 mg of frozen adipose tissue and skeletal muscle biopsies. RNA was extracted using the AllPrep RNA, DNA, miRNA Universal Kit (QIAGEN, Nordic, Solletuna, Sweden) with a DNase I (QIAGEN) digestion according to the manufacturer's instructions. The resulting DNA-free RNA samples were analyzed for quality on a 2100 Bioanalyzer according to the manufacturer's protocol (Agilent Technologies, Santa Clara, CA, USA). The RNA integrity numbers (RINs) were calculated automatically using the 2100 expert software prior to RNA sequencing.

For the RNA sequencing, we prepared the libraries using Illumina Stranded mRNA preparation and sequenced the samples on the Illumina HiSeq2000 platform to an average sequence depth of 40 to 50 M paired-ends. We sequenced adipose tissue RNA reads to a length of 75 bp and skeletal muscle RNA reads to a length of 69 bp. We aligned the reads from the samples against the human reference genome hg38 using STAR v2.5.2b and its two-pass protocol with Gencode v26 annotations.[57] We required an RNaseq sample to include at least 20 M uniquely mapped reads and the correct Library strandedness. The sample quality was assessed using Picard.[74] To avoid mixing up samples, we matched the genotype array and RNaseq data using exonic SNPs with VerifyBamID.[58] Read counts were calculated using HTSeq v0.6.1p.[59]

Skeletal muscle proteomics analysis

For the total protein extraction, we first lysed skeletal muscle biopsies of ~15 mg and homogenized in an RIPA-M buffer, followed by a full lyse in 8 M urea. The cell pellet was spun down and the supernatant discarded, and, then, the protein was washed and

precipitated with 6 volumes of acetone and stored overnight at $-20°C$. Then, we took 100 μg of protein and treated it with dithiothrei-tol and iodoacetamide to reduce and alkylate the sample, respectively, to prevent disulfide bonds. This was followed by overnight trypsinization to create peptide fragments. The resulting peptide was then cleaned with a C18 spin column (Nest Group). Further details and a step-by-step protocol for sample preparation appear elsewhere.[75] Samples were then prepared for injection on an Ab-Sciex 5600 coupled with an Eksigent LC by aliquoting 1 μg of peptide together with indexed retention-time peptides (Biognosys). The samples were then acquired in SWATH mode with 64 windows on a 60-min gradient[76] and processed using OpenSWATH v2.1.[77,78] The analysis pipeline was recently published,[78] and only briefly summarized here. Raw acquisition files (.wiff) from the mass spec-trometer were converted to mzXML using Proteowizard 3.0.5533.[65] Samples were searched with OpenSWATH v2.1 using the PanHuman library.[56] Peptides were filtered at a 1% FDR using Jumbo PyProphet v1.0. All 103 successful runs (including technical replicates) were then aligned with TRIC (in the msproteomicstools 0.8.0 package on Github), yielding 9360 proteotypic peptides cor-responding to 2935 unique proteins. Total protein levels were calculated using default parameters on mapDIA v3.0.2.[66]

Adipose tissue and muscle metabolomics

For both tissues, 20 to 80 mg of frozen tissue was homogenized under cold conditions by keeping them in a cold ethanol bath $(< -20°C)$. To homogenize the tissues, we added metallic beads and 0.5-mL cold $(-40°C)$ extraction solvent (70% (v/v) 99.9% purity ethanol in double-distilled water) to each sample and homogenized it at full speed for 1 min with TissueLyser. Thereafter, the homog-enized samples were transferred to a new tube and 7 mL of hot $(75°C)$ extraction solvent was added. The samples were incubated for exactly 1 min in a hot water bath and thorough mixing was assured through quick cycles of vortexing. After 1 min, the tubes with samples were vortexed quickly and transferred to a cold bath $(< -20°C)$. The samples were centrifuged for 10 min at 1000 g at $4°C$ and a supernatant was transferred to a new tube, whereby no liquid remained in the old tube. The metabolite extracts were dried under a vacuum at a maximum temperature of $30°C$, resuspended in 10 μL of ddH20 per mg and stored in a $-80°C$ freezer until further analysis.

Then, we analyzed the metabolite extracts through flow injection–time-of-flight mass spectrometry analysis on an Agilent 6550 QTOF instrument (Agilent) in the negative mode at 4 GHz and in the high-resolution mode in the m/z range of 50 to 1000.[79] Samples were delivered in a 60:40 mixture of isopropanol:water supplemented with NH4F at pH 9.0 at a flow rate of 150 μL/min. Ions were putatively annotated to metabolites based on an accurate mass within a 0.001-Da mass accuracy using the HMDB v3.0 database.[55] This approach allowed us to infer the molecular formula of the detected metabolites, but not to distinguish between isomers.

QUANTIFICATION AND STATISTICAL ANALYSIS

Statistical analyses

We analyzed all data using SPSS for Mac (version 24.0; SPSS Inc., Chicago, IL, USA) or R statistical programming language (version 3.3.3). In the figure and table legends, we state the specific statistical used parameters as well as the number of included twin pairs and the cutoff for statistical significance.

Participant characteristics

We assessed the anthropometric and metabolic differences between twin pairs using paired t tests for continuous variables. Skewed variables were log_e-transformed before analysis.

Proteomics and metabolomics data preprocessing

Raw proteomics data were LOESS normalized, batch corrected at the peptide level and aggregated to the protein level based on the most abundant peptide across samples. We imputed missing values by using the minimum value divided by a factor of 10. For the raw metabolomics data, we matched data across both tissues for the participant. We collapsed all duplicated samples based on the mean, followed by pareto scaling and log_2-transforming the data.[80]

Differential expression analysis

We performed differential expression analyses between co-twins using the R package Limma (Voom).[60] Prefiltering of genes was applied by retaining genes that have at least ten counts in 70% of samples and only selecting protein coding genes. We identified the altered genes, proteins and metabolites that associated with the heavier compared with the leaner co-twin within each sample. We adjusted the regression model for the sex, age group and diabetes status of the individuals. To ensure pairwise comparisons between twins, we used the family ID as the identifier. We corrected p values for multiple testing (using the Benjamini and Hochberg method) and, for the adipose tissue transcriptomics, we considered FDR $p < 0.05$ statistically significant. For adipose tissue metab-olomics and for all skeletal muscle omics analyses, applying multiple test corrections proved statistically too conservative and hampered the biological interpretation. Therefore, we considered nominal $p < 0.05$ significant for these datasets.

Biological pathway analyses

We investigated the significantly altered genes and proteins identified from the differential expression analyses using KEGG pathway enrichment analyses. For the transcriptomics results, we used the PIANO package in R and the KEGG pathways gene-set collection

CellPress
OPEN ACCESS

from EnrichR.[62] For the skeletal muscle proteomics results, we identified the KEGG pathways for the significantly differentially expressed proteins using STRING version 11.0 KEGG pathways, and considered FDR $p < 0.05$ statistically significant.

Genome-scale metabolic models

We generated genome-scale metabolic models based on the transcriptomics data to extract the so-called reporter metabolites using PIANO[61] as well as the iAdipocytes1809[63] and iMyocyte2419[64] models for the adipose tissue and skeletal muscle, respectively. These models represent a list of metabolic equations incorporated into a network that links common metabolites. The metabolic equations relate to the genes coding for each particular protein in the metabolic reaction, while reporter metabolites are also assigned to the appropriate cellular compartment. Reporter metabolites with nominal $p < 0.05$ were considered significant.

Associations with clinical variables

To analyze how mitochondrial and inflammation pathways associated with clinical variables, we calculated four mitochondrial and three inflammation pathway scores by averaging the z-scores of the associated genes in the KEGG pathways for each co-twin. We calculated the standardized beta coefficients between these four mitochondrial KEGG pathway scores, three inflammation KEGG pathway scores, selected metabolites and the clinical measures using a linear mixed-model analysis. We repeated the analysis, examining the within-pair differences in the variables, which allowed us to control for genetic influences. Family ID was used as a random factor and we adjusted the model for sex, age and diabetes status. Skewed clinical variables were $\log_e$-transformed.